The Response of the Midlatitude Jet to Regional Polar Heating in a Simple Storm-Track Model

PAOLO RUGGIERI

Centro Euro-Mediterraneo sui Cambiamenti Climatici, Bologna, Italy

FRED KUCHARSKI

Abdus Salam International Centre for Theoretical Physics, Trieste, Italy

LENKA NOVAK

California Institute of Technology, Pasadena, California

ABSTRACT

Given the recent changes in the Arctic sea ice, understanding the effects of the resultant polar warming on the global climate is of great importance. However, the interaction between the Arctic and midlatitude circulation involves a complex chain of mechanisms, which leaves state-of-the-art general circulation models unable to represent this interaction unambiguously. This study uses an idealized general circulation model to provide a process-based understanding of the sensitivity of the midlatitude circulation to the location of high-latitude warming. A simplified atmosphere is simulated with a single zonally localized midlatitude storm track, which is analogous to the storm tracks in the Northern Hemisphere. It is found that even small changes in the position of the forcing relative to that storm track can lead to very different responses in the midlatitude circulation. More specifically, it is found that heating concentrated in one region may cause a substantially stronger global response compared to when the same amount of heating is distributed across all longitudes at the same latitude. Linear interference between climatological and anomalous flow is an important component of the response, but it does not explain differences between different longitudes of the forcing. Feedbacks from atmospheric transient eddies are found to be associated with this strong response. A dependence between the climatological jet latitude and the jet response to polar surface heating is found. These results can be used to design and interpret experiments with complex state-of-the-art models targeted at Arctic–midlatitude interactions.

1. Introduction

Teleconnections emerged in scientific literature as "contemporaneous correlations between geopotential heights on a given pressure surface at widely separated points on Earth" (Wallace and Gutzler 1981, p. 784; see also Walker 1925). The atmospheric response to diabatic heating was soon recognized as a physical source of

covariance in remote areas (Hoskins and Karoly 1981). Recently, changes in the Arctic environment emphasized the potential relevance of Arctic surface forcing to the state of the global atmosphere. A crucial problem is how the midlatitude jet responds to diabatic heating and cooling at high latitudes throughout the cold season. On long time scales, Earth's surface serves as a remote forcing and an external mediator for the atmospheric circulation (Zappa and Shepherd 2017); on shorter time scales, there is growing confidence in potential predictability coming from surface conditions in high-latitude regions (Scaife et al. 2014). In both cases, the forcing can be exerted in principle by anomalous sea surface temperature, sea ice cover, and snow cover.

The complex problem posed by these premises is to understand how the atmosphere and ultimately the tropospheric jet respond to regional forcing in remote

regions of the polar cap. Causal links are not easily discernible in observations and the adjustment of the midlatitude atmosphere is likely to be small compared to the interannual variability of the system (Barnes and Screen 2015).

The second source of complexity for the pole–midlatitude teleconnections due to surface heating is in the hypothesized state dependence of the response (Overland et al. 2016) that is illustrated by the dependence of model results on the atmospheric background state (Smith et al. 2017). The perspective that is portrayed by these recent studies suggests that the deep atmospheric response to Arctic warming is modest and that state-of-the-art models are able to produce responses to Arctic surface heating that range from the positive to negative phases of the annular mode or the North Atlantic Oscillation (NAO). The positive NAO can be explained by a thermodynamic shallow linear adjustment of the lower troposphere to intensified surface heat fluxes (Deser et al. 2007; Serreze et al. 2009; Smith et al. 2017). The negative phase of the NAO can be explained by a deep response driven potentially by eddy feedbacks and by the stratosphere (Zhang et al. 2018; Ruggieri et al. 2017; Sun et al. 2015; Deser et al. 2007). Some of these studies suggest that both components are present in models, and most show that the negative NAO response is dominant (see, e.g., Deser et al. 2007; Ruggieri et al. 2017).

A possible view of the model-dependent response is that the linear shallow adjustment is always present and relatively fast. Later, it can evolve into a slower and deeper component that depends on the background state and eventually vanishes if some constraints are not met.

The insight gained by using observations and comprehensive models is limited by the availability of observations and high computational costs, as well as by the difficulty to disentangle the complex chain of mechanisms. A useful approach is to use idealized models, which create a computational laboratory, where only the essential processes for the phenomenon in question are targeted in a large number of low-cost experiments. Research on atmospheric response to high-latitude surface forcing can benefit from this idealized modeling approach.

For a surface-based Arctic warming, Cohen et al. (2014) discuss the chain of potential interactions that involves both the tropospheric midlatitude jet and the stratospheric polar vortex. In particular for the tropospheric jet, they emphasize the separation between the effect of reduced wind shear caused by a weaker equator-to-pole temperature gradient and a nonlinear interaction of the forcing with the low-level eddy-driven jet. The first mechanism suggests that the impact of Arctic warming on the jet can be explained in terms of the increase of lower-tropospheric temperature in the interior of the Arctic and the adjustment of the midlatitude jet (thermal wind balance). The second perspective points at a local dynamical interaction between eddies and temperature gradients on a smaller scale that eventually determines the shape of the jet and the meridional profile of the temperature gradient. In this case the thermal wind balance would still be maintained, but the effect of the forcing is not simply explainable in terms of thermodynamic changes of the lower-troposphere temperature. This nonlinear interaction is most likely a source of disagreement between models.

The nature of the atmospheric response to high-latitude surface heating also depends on the location of the forcing. Petoukhov and Semenov (2010) have shown that the sign of the NAO response to ice reduction in the Barents and Kara Seas is a nonlinear function of the ice cover. Sun et al. (2015) have shown that ice reduction in the Atlantic and in the Pacific have an opposite effect on the atmospheric stationary waves and consequently on the stratospheric polar vortex. Screen (2017) demonstrated that only some regions of the pole can produce a dynamical response in the atmosphere by surface heating. However, a general mechanistic understanding behind the sensitivity of the atmospheric response to the position of the high-latitude forcing is still missing.

In this study, we investigate this sensitivity in a simplified climate model. More specifically, we focus on the interaction between high-latitude heating and a localized midlatitude storm track. The investigation involves a large number of model simulations with different positions of a surface heat source. We use a similar approach to Simmons et al. (1983), who investigated tropical–extratropical teleconnections, and to Smith et al. (2010), who studied the atmospheric annular mode response to extratropical surface forcing. The sensitivity of the circulation response to the different positions of the heating relative to the climatological storm track reveals the regions where heating is particularly effective.

All experiments are comparable with realistic conditions of surface forcing in the middle and high latitudes. The model is based on the International Centre for Theoretical Physics (ICTP) AGCM dynamical core and parameterizations without land and orography, coupled to a thermodynamic mixed-layer model. The mean state of the atmosphere is zonally symmetric, apart from a perturbation introduced in the midlatitudes in the mixed-layer model. This perturbation results in a localized storm track associated with a local intensification of baroclinic processes (Kaspi and Schneider 2013). Yearlong sensitivity experiments with a secondary high-latitude heating perturbation are performed for an ensemble of atmospheric initial conditions. This idealized

framework can help us explain how the position of the surface forcing relative to the position of the storm track can modulate the magnitude of the midlatitude circulation response. Ultimately it can indicate the state dependence of the response.

Section 2 presents the formulation of the model and the design of the experiments. Results for the midlatitude response are shown in section 3, and in section 4 we discuss how the presented results can help us investigate the problem of Arctic–midlatitude interactions in high-end models. Finally in section 5 we summarize our findings.

2. Experimental design

Results presented in this study are based on simulations performed with an atmospheric general circulation model coupled to a thermodynamic mixed layer ocean model. The atmospheric model is based on the dynamical core and parameterizations of the ICTP AGCM, without orography and land. We call this configuration SPEEDY-AQUAPLANET. The atmospheric model used is described in Molteni (2003) and Kucharski et al. (2013). Model version 41 has been used at a spectral truncation of T47, with eight hybrid levels with the top of the atmosphere at 30 hPa. The thermodynamic mixed layer (slab ocean) setup is described in Sun et al. (2017). The depth of the slab ocean layer is 30 m. There is no sea ice model and, as in Voigt et al. (2016), the temperature of the water is allowed to go below the freezing point. The background Q flux used in this study corresponds to the Q flux used by Voigt et al. (2016) for the Southern Hemisphere. It has been chosen to account for a zonally symmetric midlatitude circulation. All experiments are performed with perpetual equinoctial conditions.

To induce a localized storm track in the midlatitudes, we introduce a perturbation in the ocean Q flux. This perturbation is based on the setup that Kaspi and Schneider (2013) used to look at the role of stationary eddies to define the shape of midlatitude storm tracks. The rationale for this setup is to locally sharpen the midlatitude temperature gradient in order to amplify baroclinic instability, which ultimately produces a zonally confined storm track that resembles storm tracks in the Northern Hemisphere. In addition to this midlatitude Q-flux forcing, secondary Q-flux perturbations are applied in the high latitudes to simulate surface diabatic heating from the ocean to the atmosphere, as described in the following subsections.

a. SPIN-UP experiment

This experiment was performed to generate a distribution of equilibrated atmospheric states with a zonally

symmetric Q flux (Q_{Sym}). Our estimate of the spin-up time of the system is smaller than 10 years (not shown). This simulation has been initialized from a state equilibrated with the standard version of the model (with continents and orography).

b. ZONAL experiment

The ZONAL experiment is run with Q_{Sym} (i.e., as in SPIN-UP) but restarting the model from initial conditions obtained from SPIN-UP. This experiment was used as a reference for a zonally symmetric climate. It is 70 years long, and the first 20 years were not used in the analysis or used to restart any other simulation.

c. TRACK experiments

TRACK experiments are identical to the ZONAL one, except for the introduction of the midlatitude perturbation (hereafter Q_{Track}), which is added to Q_{Sym}. As pointed out previously, the perturbation that was introduced is based on Kaspi and Schneider (2013) and it is applied by a triangular area of enhanced Q flux in the jet region between 25° and 50°N, and between 50° and 80°E. The value of Q_{Track} is set constant over the triangle (at 450, 225, and 112.5 W m^{-2}, respectively, for TRACK0, TRACKa, and TRACKb) and equal to a negative value elsewhere in that latitude band, to ensure that no net heat is supplied to the atmosphere. Figure 1 shows climatological fields from the TRACK0 experiment. The shape of the perturbation in the sea surface temperatures resembles closely the pattern of the imposed Q flux. The transient heat fluxes are concentrated into a single storm track, which is qualitatively similar to the North Atlantic and North Pacific storm tracks. The perturbation in the jet is detectable in both the lower and upper troposphere. The climate of the TRACK0 atmosphere is dominated by a wavenumber-1 structure of the jet, with substantial deviations from the zonal average.

d. CONTROL experiments

The CONTROL experiments are used as reference states for all the experiments with the additional high-latitude heating. They are equivalent to the respective TRACK experiments minus the first 20 years of the integration (e.g., CONTROL0 corresponds to the last 50 years of the TRACK0 simulation, and CONTROLzonal to the last 50 years of the ZONAL experiment).

e. HIGH-LATITUDE HEATING experiments

The setup of this set of experiments is shown synthetically in Fig. 2. They are performed with the same setup as CONTROL, but with an additional high-latitude heating, switched on at the beginning of the simulation. This high-latitude heating is 6 times smaller than the total heating imposed by the midlatitude triangle.
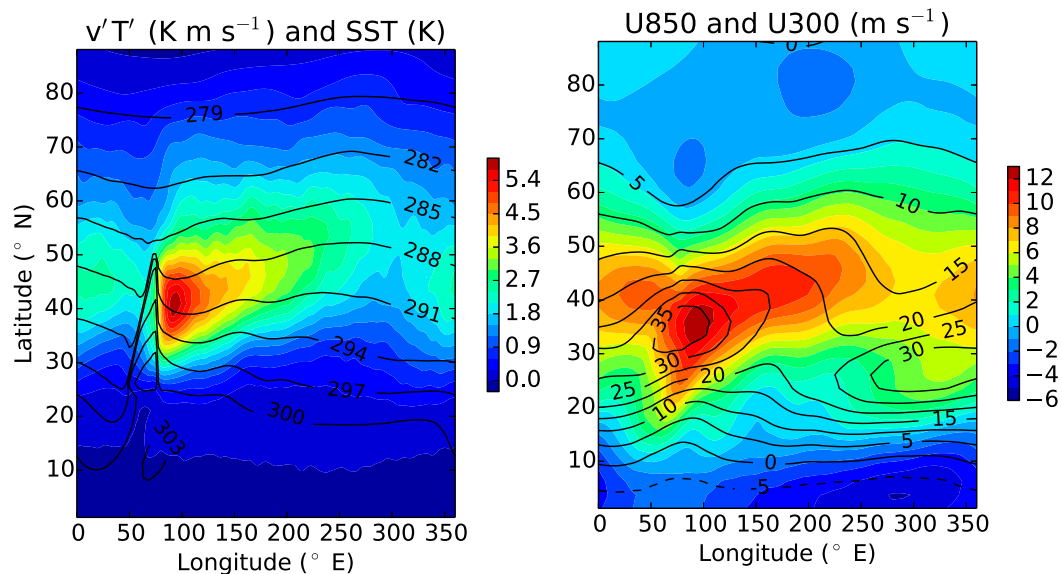
FIG. 1. Plots of fields from the TRACK0 experiment. (left) Sea surface temperatures (contours; K) and transient eddy heat flux at 850 hPa (colors; K m s^{-1}). (right) Zonal wind at 300 (contours; m s^{-1}) and 850 hPa (colors; m s^{-1}).

The initial conditions are obtained from CONTROL at day 1 and every 365 days.

Three subsets of experiments are labeled: northern (N; 67.5°N), central (C; 65°N), and southern (S; 62.5°N). In these cases the latitude of the heating is fixed but the longitude is varying. Individual experiments in this set are labeled with numbers between 0 and 360 to indicate the longitude of the center of the heating area. Three subsets of experiments are labeled with two numbers: the first indicating the longitude (which is kept fixed) of the heating and the second indicating its latitude (which is varied); for example, exp_250_67.5 is equivalent to exp_N250. In these cases the longitude of the heating is fixed but the latitude is varying.

The spatial pattern of the additional heating Q_h is defined by

$$Q_h(\lambda, \phi) = \begin{cases} A\exp\left[-\dfrac{(\phi - \phi_0)^2}{\sigma_\phi^2} - \dfrac{(\lambda - \lambda_0)^2}{\sigma_\lambda^2} \right] & |\phi - \phi_0| \leq 7.5°, |\lambda - \lambda_0| \leq 15°, \\ 0 & \text{elsewhere}, \end{cases} \quad (1)$$

where ϕ is latitude, λ is longitude, $\sigma_\phi = \sqrt{32}°$, and $\sigma_\lambda = \sqrt{162}°$. The value of A is chosen to ensure that

$$I_h = \int_{\phi_0 - 7.5°}^{\phi_0 + 7.5°} \cos(\phi)\, d\phi \int_{\lambda_0 - 15°}^{\lambda_0 + 15°} d\lambda\, Q_h(\lambda, \phi) = 75\,\text{W m}^{-2}\,\text{rad}^2 \quad (2)$$

and thus the parameter A increases with latitude. The choice of conserving the angular extent and the total intensity I_h implies that the spatial scale of the heating becomes smaller at higher latitudes. Ultimately the Q flux used in this set of experiments is

$$Q_{\text{TOTAL}} = Q_{\text{Sym}} + Q_{\text{Track}} + Q_h(\lambda_0, \phi_0). \quad (3)$$

The average perturbation of the sea surface temperature induced by Q_h, measured as the average over the heating area defined by Eq. (1), ranges from 1.4 K in month 1 to 8.3 K in month 12, being 7.5 in month 6. In series N, C, and S the anomalous sea surface temperature south of 45°N is always below 0.25 K (in the ensemble mean), in all experiments and at any lead time. The anomalous net surface heat flux from the ocean to the atmosphere in the heating area, averaged between month 1 and month 12, is about 70.5 W m^{-2}.

A small systematic response of the sea surface temperature to latitudinal shifts in the high-latitude forcing is found in the N, C, and S experiments, with the differences being about 4% of the mean response. A third set, in which experiments are labeled Z0, Za, Zb, and Zc, is performed with a heating applied uniformly across the polar cap (65°–90°N). In these experiments the total heat supplied is also equal to I_h.
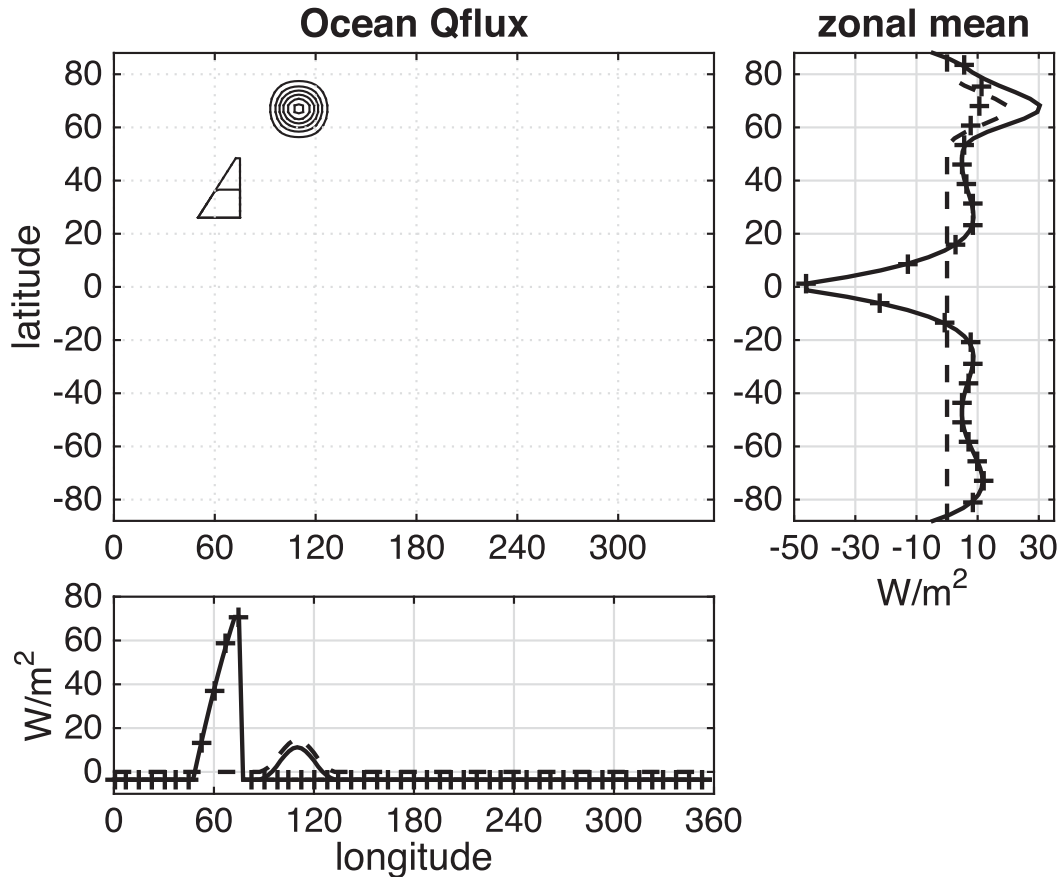
FIG. 2. Illustration of the experimental setup. (top left) The Q flux used for experiment N109. (bottom left) The meridional average and (right) the zonal average of the Q_{TOTAL} (solid line), Q_{Track} (crosses), and Q_h (dashed line). Note that the zonal mean of Q_{Track} is equal to that of Q_{Sym}.

All experiments are compared with CONTROL0 with the exception of Za, Zb, and Zc, which are compared respectively with CONTROLa, CONTROLb, and CONTROLzonal. The positions of the heating, labels, and other details are summarized in Table 1. Each additional heating experiment is a 50-member, 1-yr-long integration, starting from initial conditions obtained from a previous model run. Model output of high-latitude heating experiments is made of 2150 years (out of the total 2550 years) with 43 different combination of forcing and mean state.

3. Results

a. The atmospheric response to mid- and high-latitude heating

The setup presented in section 2 was used to perform 43 model experiments, where localized heating of the polar cap was shifted latitudinally and longitudinally. In the names of the experiments letters N, C, and S refer

to the northern, central, and southern latitude of the heating, respectively (as detailed in Table 1), and numbers refer to the longitude of the heating. Experiments with a zonally symmetric heating (applied between 65° and 90°N) are labeled with the letter Z. The average response of all experiments with high-latitude heating (series N, C, and S) is shown in Fig. 3a. This figure shows that a surface warming affects primarily the poleward flank of the climatological jet (roughly confined in the 55°–80°N band), with its magnitude being smaller than 1 K. The jet response is strongest near the storm track, with the jet being displaced equatorward and weakened. The mean responses are small compared to the mean values of zonal wind and compared to the variability of the system. The jet response is similar at 850 hPa (not shown). The average response of the localized heating experiments is weaker but comparable to the response of the experiment with a zonally symmetric heating (Fig. 3b).

To investigate the spread in the responses of different experiments, Fig. 4 shows time series of four diagnostics

TABLE 1. Summary of model runs. From left to right, columns show the label that identifies a series of experiments, whether they have a localized storm track and/or an additional heating, the position of the additional heating if present, the size of the ensemble and the length of the integration, the number of experiments in the series and the restart data. Experiments Z0, Za, and Zb are restarted, respectively, from TRACK0, TRACKa, and TRACKb. Note that three experiments counted in series 15, 109, and 250 are identical to some experiments of series N, C, and S.

	Surface forcing		Position of heating		Ensemble size (length in years)	No. of experiments	Initialized from
Label	Storm track	Heating	λ_0 ($k = 0, \ldots, 7$)	ϕ_0 ($k = 0, \ldots, 2$)			
SPIN-UP	No	No	—	—	1 (70)	1	SPEEDY
ZONAL	No	No	—	—	1 (70)	1	SPIN-UP
TRACK0, TRACKa, TRACKb, TRACKzonal	Yes	No	—	—	1 (70)	3	SPIN-UP
CONTROL0, CONTROLa, CONTROLb, CONTROLzonal	Yes	No	—	—	1 (50)	3	SPIN-UP
N	Yes	Yes	15°E + $k47°$	67.5°N	50 (1)	8	TRACK0
C	Yes	Yes	15°E + $k47°$	65°N	50 (1)	8	TRACK0
S	Yes	Yes	15°E + $k47°$	62.5°N	50 (1)	8	TRACK0
15	Yes	Yes	15°E	50.5°N + $k5°$, 62.5°N + $k5°$, 65°–70°N	50 (1)	8 (5)	TRACK0
109	Yes	Yes	105°E	50.5°N + $k5°$, 62.5°N + $k5°$, 65°–70°N	50 (1)	8 (5)	TRACK0
250	Yes	Yes	245°E	50.5°N + $k5°$, 62.5°N + $k5°$, 65°–70°N	50 (1)	8 (5)	TRACK0
Z0, Za, Zb, Zc	Yes	Yes	—	Applied north of 65°N	50 (1)	4	TRACK0, TRACKa, TRACKb, ZONAL

analyzed for the N, C, and S experiment series. Dashed gray lines denote the individual experiments and the solid line denotes their mean. The blue dashed line corresponds to the experiment Z0 whose response is not significantly different from the mean of the experiments with localized heating, agreeing with Fig. 3. We also highlight experiment N250 (red dashed line), which produces the strongest response in geopotential height and low-level wind, which are related to the eddy-driven part of the circulation response (e.g., Woollings et al. 2010). We see that as the ocean warms the atmosphere, the temperature of the polar cap grows on average monotonically up to about 1 K (Fig. 4a). The magnitude of the 300-hPa zonal wind in the extratropical Northern Hemisphere (Fig. 4b) is less sensitive than the temperature but nevertheless decreases on average monotonically, with all experiments producing weaker zonal wind after month 6. This is broadly consistent with the adjustment to thermal wind balance. The increase in the 300-hPa geopotential height over the polar cap (Fig. 4c), an indicator of the phase of the annular mode, is also consistent but shows less sensitivity than the other two fields. The high-latitude zonal wind (Fig. 4d) shows a weak and slower negative signal. A similar result is found in the high-latitude zonal wind at 850 hPa (not shown).

Focusing in particular on Fig. 4b, the impact of the heating on the jet speed (dominated in our diagnostic by the thermally driven jet) is rather small but present in all experiments. In contrast, the response of the eddy-driven component (which is arguably dominant in Figs. 4c and 4d) can reach significantly high values in some cases, but on average it is not statistically distinguishable from noise. The thermal wind balance is insufficient to explain these high-latitude circulation responses.

An interesting question is, What is responsible for the large spread of circulation responses compared to the relatively small spread of temperature responses seen in Fig. 4? To address this question we show results for two experiment series that are particularly illustrative of the relationship between the position of the forcing and the response, namely, series N (constant latitude, varying longitude) and series 250 (constant longitude, varying latitude). These two series have been selected because their intersection corresponds to the location of the forcing in experiment N250 (red line in Fig. 4), which yields a particularly strong response.

The 850-hPa zonal wind for the four experiments in series N is shown in Fig. 5. The low-level wind field has been used since anomalous patterns are dominated by the deep eddy-driven component of the jet, but the
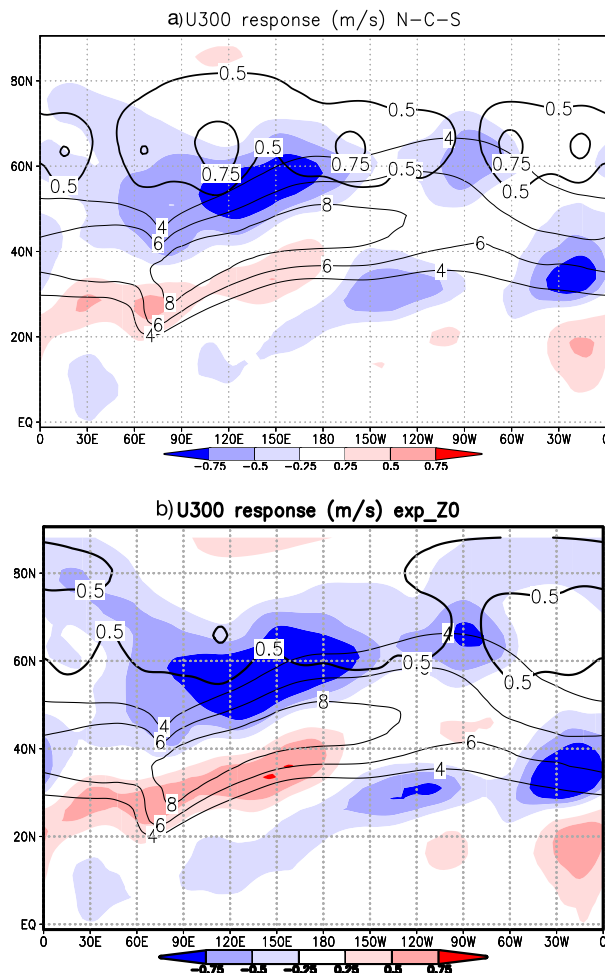
FIG. 3. (a) Climatological zonal wind at 850 hPa (thin contours; m s^{-1}), anomalous zonal wind at 300 hPa (shading; m s^{-1}), and anomalous temperature at 850 hPa (thick contours; K). The climatology is computed from the time mean and ensemble mean of CONTROL0. Anomalies are computed for fields averaged from month 1 to month 12 and averaged for all the experiments in the series N, C, and S (see Table 1 for details). (b) As in (a), but for the individual Z0 experiment.

300-hPa wind yields similar results (not shown). Starting from Fig. 5a, when the heating is applied poleward of the triangular storm-track forcing, the temperature gradient weakens slightly downstream of the storm track. A quadrupolar anomaly is found in the wind across the hemisphere, indicating enhanced poleward tilting of the jet. When the heating is placed farther downstream toward the terminus of the jet maximum (Figs. 5b,c), the jet response becomes stronger and less tilted, resulting in an annular latitudinal shift in the jet. When heating is near the jet exit (Fig. 5c), the hemispheric response is very strong in the high latitudes and shows an equatorward shift of the jet. When the heating is

placed upstream with respect to the storm-track triangle (Fig. 5d), the midlatitude response is very weak and local.

In general the magnitude and nature of the response depend strongly on the zonal coordinate, and when the heating is downstream, but far from the midlatitude storm track, the response reaches its maximum magnitude and spatial extent.

The corresponding results for the six experiments of series 250, where the latitude is varied and longitude is fixed, are shown in Fig. 6. The heating is moved from the interior of the jet (Fig. 6a) up to the poleward flank of the jet (Fig. 6f). The strongest responses are found for the northernmost and southernmost positions of the heating and project onto the positive and negative phases of the annular mode. The intermediate positions produce weaker (in the zonal-mean sense) and more localized responses. Figures S1 and S2 in the online supplemental material show the analogous fields for series N15 and N109. It is apparent that the magnitude of the response to high-latitude heating, compared to lower-latitude heating, is much more dependent on the longitude of the heat source.

To demonstrate the sensitivity to the location of the heating more explicitly, Fig. 7 summarizes results from all localized-heating experiments (solid lines), as well as the experiment with zonally symmetric heating (Z0; dashed line). The localized-heating experiments are grouped into the S, C, and N series in Fig. 7a, and into series 15, 109, and 250 series in Fig. 7b. For series S the response is detectable primarily in the storm-track area. When the heating is moved poleward, the peak of the response becomes largest for experiments with heating longitudes farther away from the storm track. The sensitivity to small changes in the latitude of the forcing is weak or moderate in the proximity of the storm-track sector, but far downstream it becomes very large (where the response ranges from 0 to the maximum value detectable in these diagnostics).

In Fig. 7b, we show the same index shown in Fig. 7a for series 15, 109, and 250. In this case the three series correspond to the heating being far from the storm track (series 15), at the beginning of the storm track (series 109), and in the jet exit region (series 250). In each series, the longitude of the heating is fixed, while the latitude is varied. When the heating is placed in the 50°–55°N band, the response of the jet always projects onto the positive phase of the annular mode. The two profiles start diverging as the heating is placed in the polar regions (60°–70°N). For series 250 (where the heating is downstream of the storm track), the index shows a very narrow neutral band and reaches strongly negative values, decreasing almost monotonically with increasing
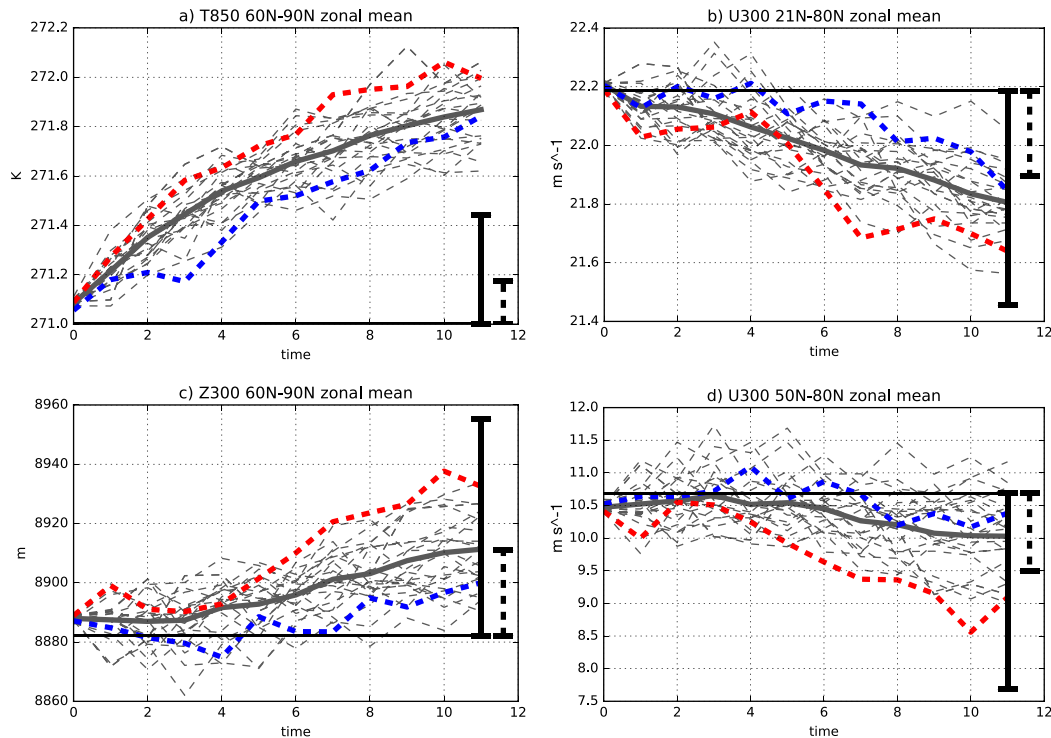
FIG. 4. Monthly time series for the N, C, and S experiments. Each line in these plots is the ensemble mean of the 50-member ensembles initialized from TRACK. In each panel the red line is the experiment N250, the blue line is the experiment Z0, and the gray dashed lines are all other experiments in the high-latitude heating set. The solid gray line is the average of all dashed gray lines. Fields displayed are (a) temperature at 850 hPa over the polar cap, (b) zonal wind at 300 hPa between 21° and 80°N, (c) geopotential height at 300 hPa over the polar cap, and (d) zonal wind at 300 hPa between 50° and 80°N. The black solid horizontal line is a measure of the climatological reference value for the quantity displayed that has been obtained from the CONTROL0 run. The interval marked by the solid vertical black line corresponds to one month-to-month standard deviation of the index in the CONTROL0 run. The dashed vertical black line shows the maximum change of the mean of the distribution that is not statistically significant at 95% confidence level, assuming that the standard deviation of the index is not perturbed (98 degrees of freedom have been assumed and a Student's t test has been used).

latitude. For series 109 (where the heating is placed in the proximity of the storm track) the index is insensitive to latitude changes in the polar cap and the response converges to the response to a zonally symmetric forcing. Finally, for series 15 the index shows smaller negative values in the 60°–70°N band, but converges slowly toward to the response of Z0. When the heating is placed farther north, the response is slightly larger than that of the zonally symmetric forcing of Z0.

b. Analysis of eddy feedbacks

Figure 8a shows that, on average, the surface warming in the polar regions reduces the storminess, with the reduction being most pronounced in the storm-track region (Fig. 8a). In some experiments the storm track is shifted farther north and its zonal extension is reduced (e.g., exp. N344 in Fig. 8b). In other cases, for instance experiment N250, in Fig. 8c, the storm track responds with a shift toward midlatitudes and a reduction of intensity in the high latitudes. Figures 8d and 8e show that the response in storm-track intensity and latitude is proportional to the response in zonal wind speed. Analysis of changes in Eady growth rate in the lower troposphere (not shown) revealed that the reduction of storminess is unlikely to be due to reduced baroclinicity in the region of strong heat fluxes shown in Fig. 1 (in the proximity of the triangle), as may have been expected from the reduced equator-to-pole temperature gradient. Instead, storm tracks are modified primarily away from the baroclinic zone, more locally relative to the high-latitude heating.

To explore the source of variability in the response to changes of the longitude of the high-latitude heat, we concentrate on the N series and investigate the eddy effects on the mean-flow acceleration. In particular we study the Eliassen–Palm flux (EP flux) divergence, which signifies acceleration of the mean flow (Edmon
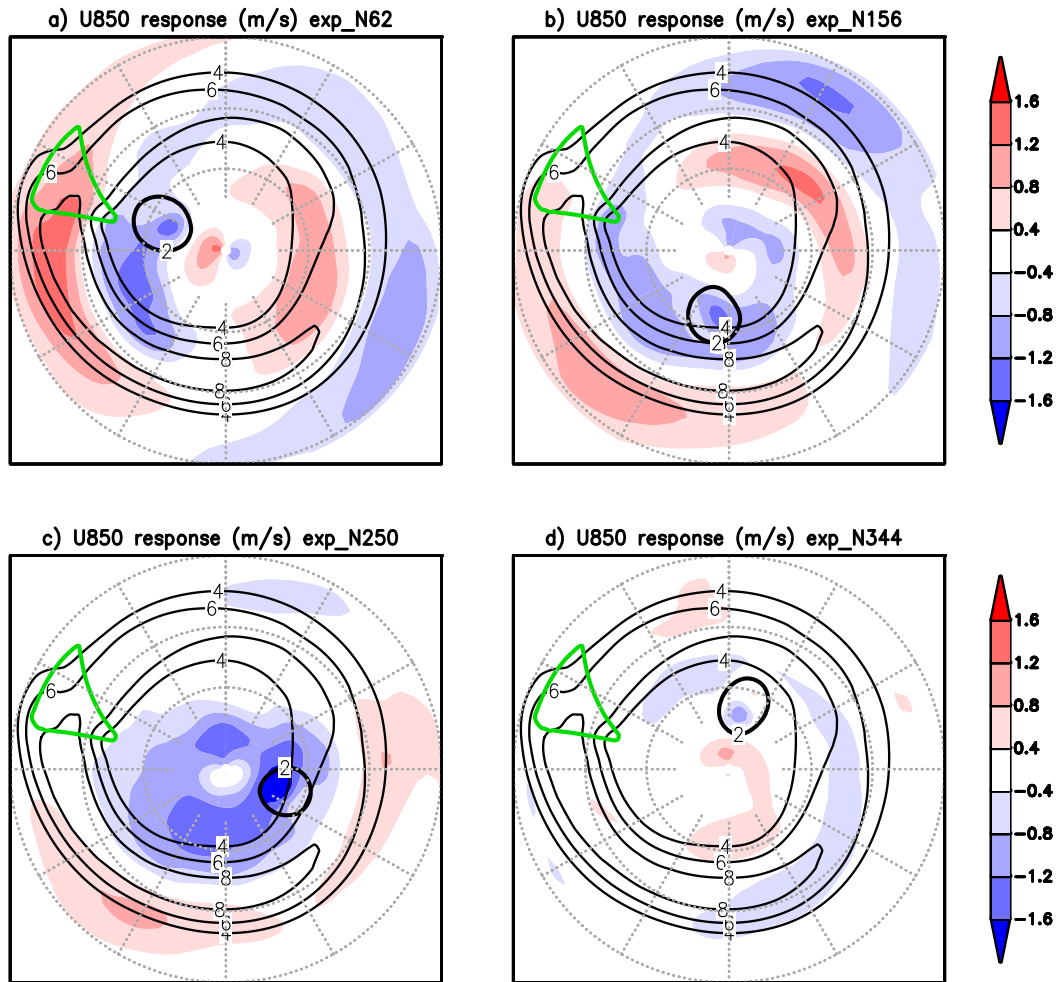
FIG. 5. Climatological zonal wind at 850 hPa in CONTROL0 (thin black contours) and anomalous zonal wind at 850 hPa (colors; m s^{-1}) averaged from month 4 to month 12 for experiments (a) N62, (b) N156, (b) N250, and (d) N344. A thick black contour drawn at 2 K indicates anomalous temperature at 850 hPa. A green contour indicates the position of the storm-track triangle.

et al. 1980). We then separate the EP flux and its divergence into linear and nonlinear components, and into transient and stationary components. The method for the computation of the heat fluxes, momentum fluxes, zonal wind tendency, and the decomposition into the different EP-flux components is outlined in the appendix. It was found that the anomalous divergence of the EP flux in the upper troposphere is dominated by the convergence of momentum flux. Hence we present only the zonal wind tendency explained by momentum flux convergence at 300 hPa as an indicator of eddy feedbacks on the tropospheric jet, and the heat flux at 100 hPa as an indicator of the response of the annular mode (and the stratosphere).

The climatological zonal wind and EP flux and the anomalous EP flux divergence for one experiment

(N250) are presented in the supplemental material (Fig. S3).

Figure 9a shows that in the eight experiments of series N, the zonal-mean zonal wind response at 300 hPa ranges from near 0 to about −0.5 m s^{-1}. Similarly, the tendency explained by the momentum flux convergence peaks in the latitudinal band where the heating is applied. Below we therefore refer to the momentum flux convergence as eddy-induced tendencies of zonal wind (or eddy tendencies in short). If the eddy tendency (brown line in Fig. 9a) is averaged between 50° and 80°N, it displays a range of values from slightly positive to strongly negative (Fig. 9b). It is evident that the magnitude of the zonal-mean jet response in the upper-troposphere is proportional to the eddy tendency. When the eddy tendency is separated into the linear and
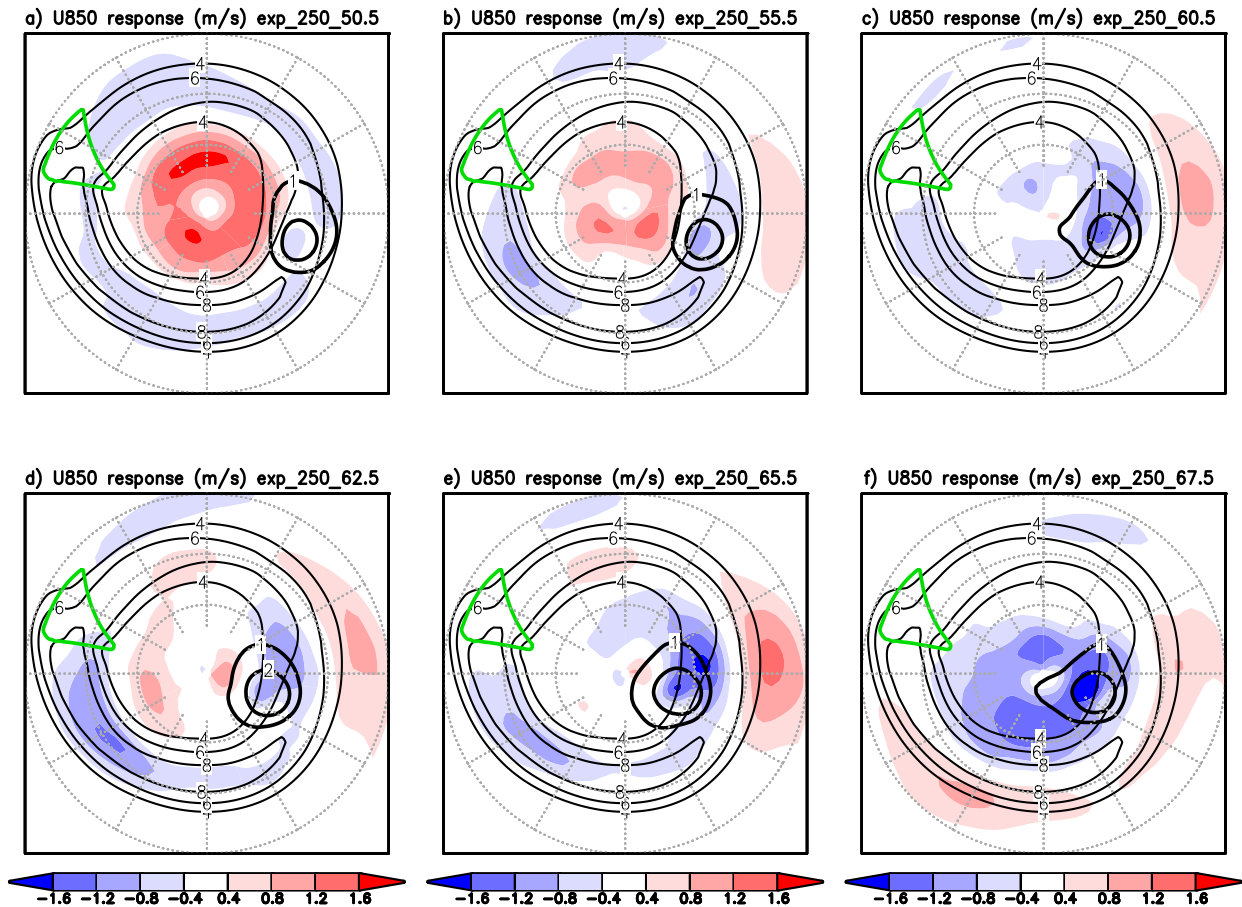
FIG. 6. As in Fig. 5, but for series 250. Two thick contours, drawn at 1 and 2 K, are used for temperature at 850 hPa.

nonlinear components (Figs. 9c,d), it is apparent that this proportionality with the jet response is mainly due to the nonlinear component (Fig. 9d). The feedback from nonlinear eddies ranges from positive to negative and, if only transient eddies at synoptic frequencies are considered, a similar linear relationship is found (Fig. 9e), but in this case the eddy tendency is on average negative. Note that the linear component of the anomalous tendency corresponds to the linear interference between the climatological waves and the zonally asymmetric component of the response. Although this interference term acts to decrease the total tendency, it is not proportional to the jet response. It can be concluded that the magnitude of the tendency by momentum fluxes in the upper troposphere associated with transient eddies modulates the magnitude of the jet response.

Figure 9f shows the dependence of this relationship on the longitude of the applied heating. To stay concise, we only show the whole nonlinear (transient plus stationary) momentum flux convergence, and the nonlinear transient momentum flux convergence. It is apparent that the eddy

forcing on the zonal wind tendency is strongest for experiments where the heating forcing is far downstream of the storm track (peaking at 250°E). The transient eddies therefore may be responsible for the heating applied in experiment N250 having such a strong impact. The heating placed downstream with respect to the midlatitude heat source and thus in coincidence with the area of poleward propagating storms produces stronger (more negative) transient eddy feedbacks. This panel also shows the lower-stratospheric linear temperature flux, and the lower-stratospheric total temperature flux (linear plus nonlinear). The temperature fluxes are most responsive if the heating is applied slightly downstream of the storm track (positive response) or just upstream of it (negative response). However, anomalous propagation of waves above the tropopause and the component explained by linear interference do not explain the strong jet response in the experiments where the heating was applied near the jet exit (e.g., the N250 experiment).

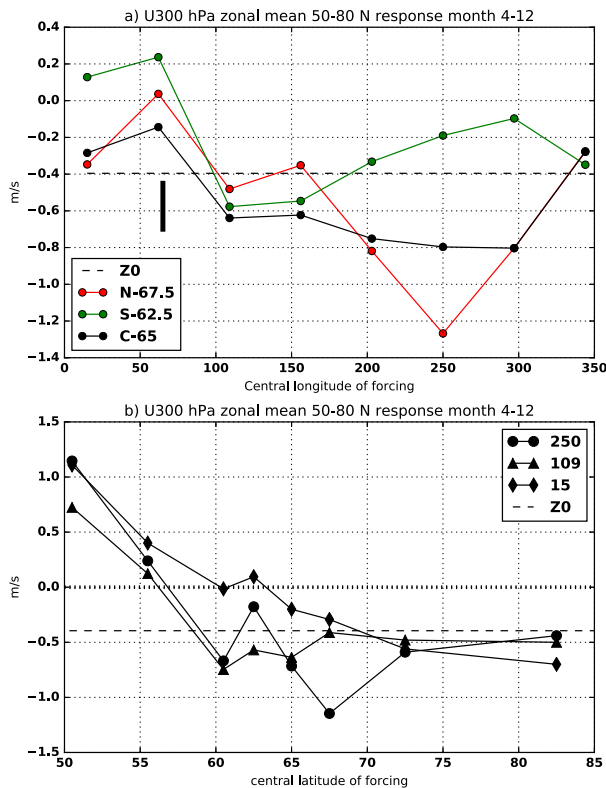While the average response is stronger and partly confined to the core of the storm track, experiments

FIG. 7. (a) High-latitude zonal wind response at 300 hPa for months 4–12 and zonally averaged for series N, C, and S (solid lines) and for Z0 (dashed line). A thick vertical line at 65°E marks the central longitude of the storm-track triangle. (b) As in (a), but for series 109, 250, and 15 (solid lines) and for Z0 (dashed line).

differ mostly in the downstream region. This fact can be inferred from Fig. 5 but is shown explicitly by Fig. 10. This figure shows the regression coefficient between the eddy-induced nonlinear zonal-mean tendency (calculated as in Fig. 9d) as the predictor and the zonal wind (a horizontally varying field) as the predictand. The strong zonal-mean response is associated with a stronger change (equatorward displacement and peaked easterly anomaly on the poleward side) in the nonlinear eddy effects on the downstream side of the tilted jet. The proximity of a heat source to the poleward flank of the jet is key to establish a strong response in this area. It should be noted that these results are not corroborated by statistical tests on the goodness of the fit, but they are able to provide sufficiently clear indications about the relationship between the jet response and the EP-flux components.

To test the dependence of the response on the background state we changed the climate of the simple system by multiplying the triangular heating (and the associated cooling, which ensures that the zonal-mean heating of the triangle forcing is zero) by a multiplicative

factor and we repeated the experiment with the zonally symmetric high-latitude heating (Z0). Results from these additional experiments are shown in Fig. 11. When the magnitude of the heating is reduced, the tilt of the jet is also significantly reduced but the mean latitude of the low-level jet is shifted poleward by a few degrees. Interestingly, in the model with zonally symmetric climate (i.e., when the midlatitude perturbation is not applied), the average response is very close to zero, whereas when the jet is perturbed, being shifted poleward and tilted, the response becomes stronger. A larger tilt that comes, in our setup, with a more equatorward position of the jet on average, is less prone to produce a response to a zonally symmetric forcing and a large sensitivity to the longitudinal position of the heating that eventually produces a strong response in some cases.

4. Discussion

The setup presented in section 2 has been used to perform 43 experiments, which were designed to target the dynamical response of the midlatitude circulation to high-latitude diabatic heating at the surface. The simplified setup allowed us to systematically change the position of the heating in longitude and latitude. This in turn allowed us to construct a sensitivity map of the responses to the heating location.

The choice of an aquaplanet simplifies the setup and the analysis in many aspects. 1) A uniform water surface means that the response is unaffected by sharp land–sea thermal contrast within the planetary boundary layer (see, e.g., Petoukhov and Semenov 2010). 2) Considering the nature of the stationary upper-tropospheric waves, this setup simplifies also the troposphere–stratosphere feedbacks. Indeed, the lack of strong zonal asymmetries suppresses variability in the stratosphere and weakens potential interactions between the response and the climatological waves (not shown) that have been documented by many studies (Sun et al. 2015; Ruggieri et al. 2017; Zhang et al. 2018). 3) The perpetual equinoctial condition allows study of the temporal evolution of the response without the interference of the seasonal cycle. This simplification is particularly useful when considering phenomena of time scales comparable to the seasonal cycle. Otherwise, seasonal changes in the average jet position and variability would introduce further complications.

Although these simplifications help isolate the atmospheric adjustment to high-latitude surface heating, they also introduce caveats to be born in mind when interpreting the results in the context of the atmospheric dynamics on Earth. Most importantly, the absence of realistic topography and land–sea contrast may weaken
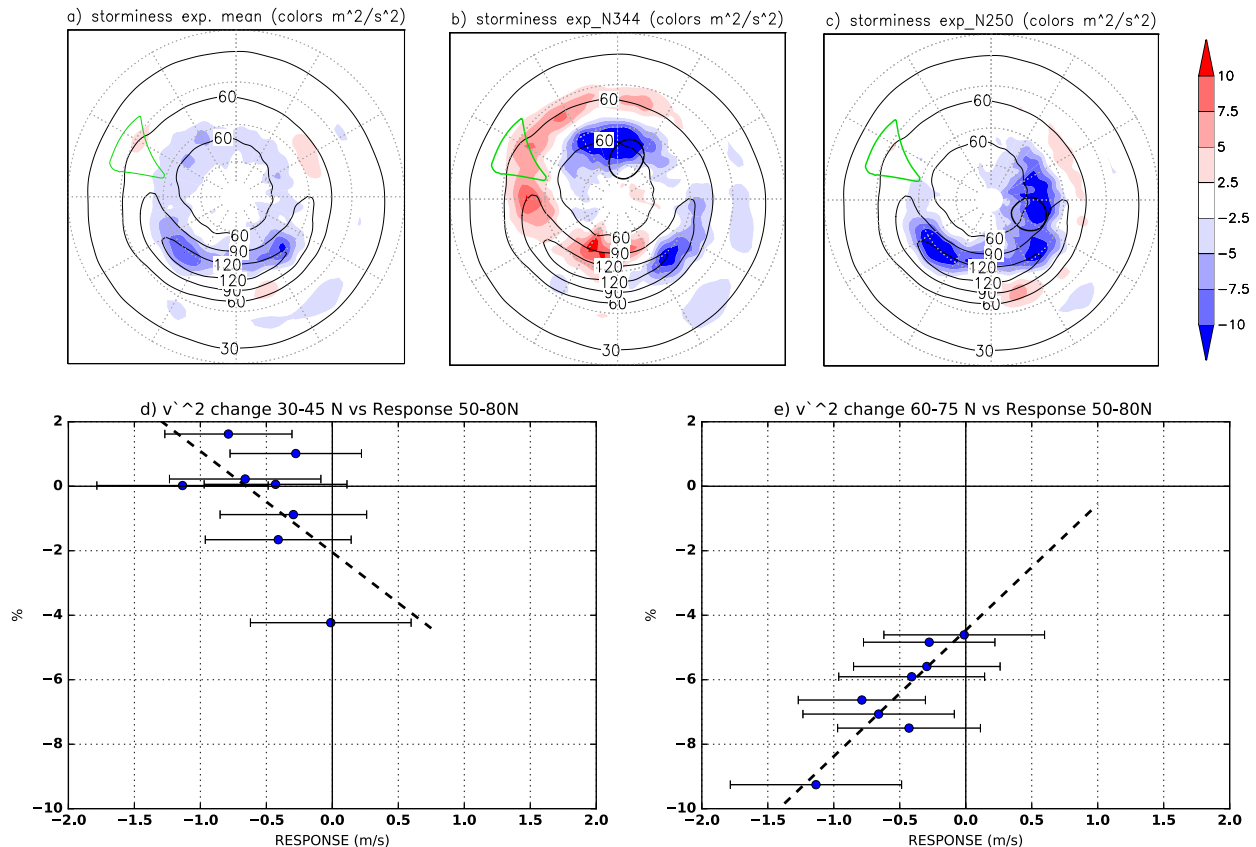
Fig. 8. (a) Climatological values of storminess v'^2 ($m^2\,s^{-2}$; thin contours) and average anomaly of experiments of series N ($m^2\,s^{-2}$; colors). A green contour indicates the position of the storm-track triangle. (b) As in (a), but for experiment N344 and a thick contour indicates the location of the heat source. (c) As in (b), but for experiment N250. (d) Jet response at 300 hPa (50°–80°N) vs percentage change of storminess in the midlatitudes (20°–45°N). (e) As in (d), but in the high latitudes (50°–80°N). Storminess is defined as the variance of transient meridional velocity and in (d) and (e) it is expressed as percentage of the corresponding climatological value in CONTROL0.

the interaction between mean flow and anomalous flow. On Earth, and especially in the Northern Hemisphere, the effect of linear interference is expected to be stronger (e.g., Sun et al. 2015). It should also be noted that we impose heating only at the surface, but the sensitivity to the depth of the heat source may be also be significant (see, e.g., Sellevold et al. 2016). Similarly, in our case the temperature perturbation is confined below 500 hPa (not shown), while the seasonal cycle of the depth of the perturbation may be large, producing deeper perturbations in summer and vice versa in winter. Cloud feedbacks and anomalous latent heat release in the midtroposphere are not significant in our case (not shown).

The present study emphasizes the midlatitude response of the circulation to polar surface heating by the adjustment of the tropospheric jet. The focus of the analysis is the comparison between experiments with different heat sources. Overall the response is

weak compared to the mean state and variability of the system, but the idealized model has allowed us to perform a large number of simulations (50 per experiment), which is sufficient to provide statistical significance even for the small responses. Additionally, for some specific experiments the response can become comparable with the variability of the system.

Along these lines, more emphasis is placed on the sensitivity to the location of the heating (Figs. 4–7; see also Figs. S1 and S2) rather than on the fact that the system on average responds as shown in Fig. 3. Nonetheless, despite the simplicity of the system, the dynamical response of the jet, when present, falls in the case described by Smith et al. (2017), with enhanced EP-flux divergence toward the equatorward side of the jet and vice versa on the poleward side. The upward flux above the tropopause does not seem to be related to the magnitude of the jet response. Moreover, the
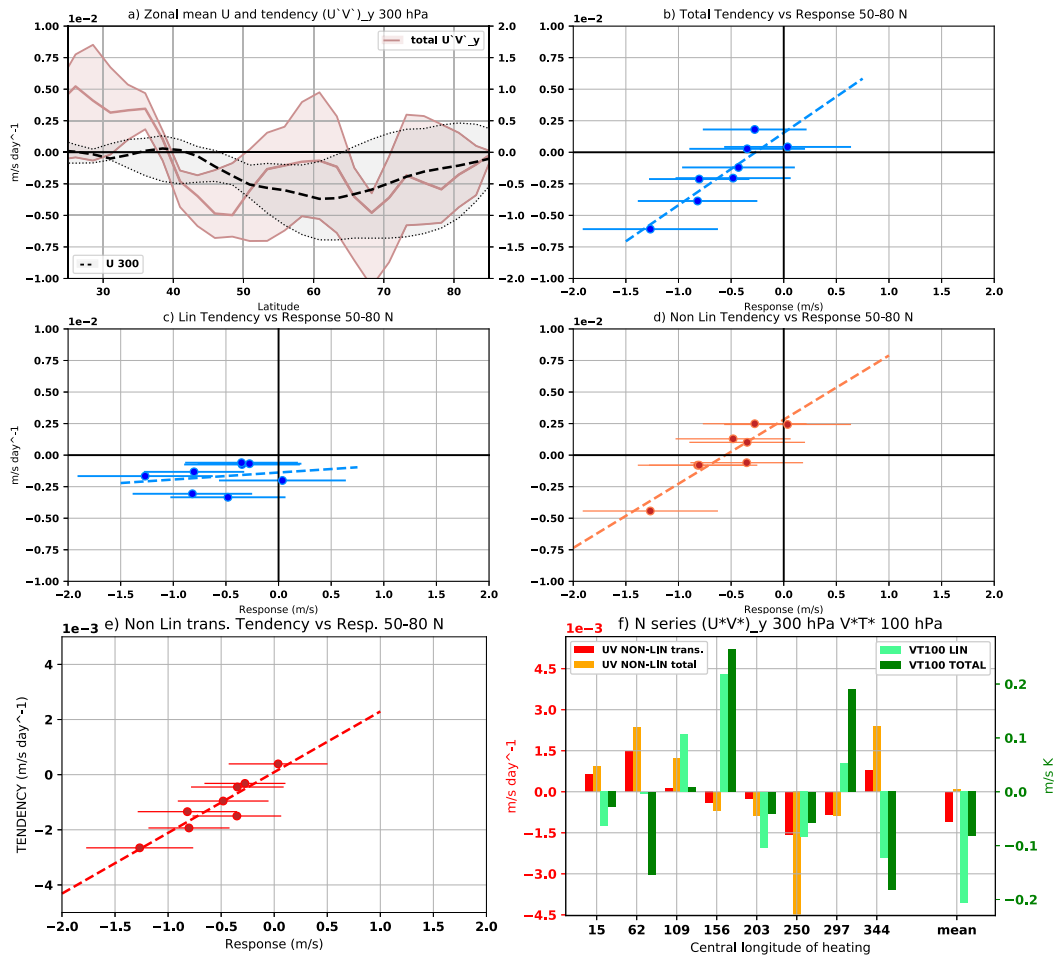
FIG. 9. (a) Median, maximum, and minimum values in N series of the total momentum flux convergence anomaly (solid; m s^{-1} day^{-1}; left axis) and of anomalous zonal wind (dashed; m s^{-1}; right axis) at 300 hPa and zonally averaged. Anomalies are computed by averaging between months 4 and 12 and subtracting the climatology of CONTROL0. Note that in these experiments the central latitude of the heating is fixed. (b) Relationship between the momentum flux convergence shown in (a) averaged between 50° and 80°N and the response of the zonal-mean zonal wind at 300 hPa defined as in (a). (c) As in (b), but for the linear component of the momentum flux convergence. (d),(e) As in (b), but for the nonlinear component and for the nonlinear component of transient synoptic eddies, respectively. See appendix for exact definition of linear and nonlinear components. Bars indicate the interval where the response is not statistically significant at 95% confidence according to a Student's *t* test. (f) Summary of nonlinear momentum convergence (total and transient synoptic eddies in yellow and red, respectively) at 300 hPa and total and linear eddy heat flux at 100 hPa (dark green and light green, respectively). Values are deviations from the multi-experiment mean that is displayed toward the right side of (f). Note the different *y* axes.

dependence of the magnitude of the response on the climatological latitude of the jet also agrees with Smith et al. (2017). The relationship with the climatological refractive index of Rossby waves has been examined in our experiments (not shown). There are indications that, as in Smith et al. (2017), the difference between the high- and low-latitude refractive indices can modulate the magnitude of the response to surface heating in the poles, by a modulation of the preferred propagation of waves. However, in our dataset this result is

not robust and depends strongly on the choice of the averaging sectors.

It is emphasized here that, as noticed by McKenna et al. (2018), the tropospheric circulation response to polar surface heating resembles the negative NAO or, more generally, an equatorward shift of the midlatitude jet. This is the circulation response, regardless of the longitudinal position of the high-latitude heating. Some studies (e.g., Sun et al. 2015) have found that the stratosphere responds in an opposite way when the
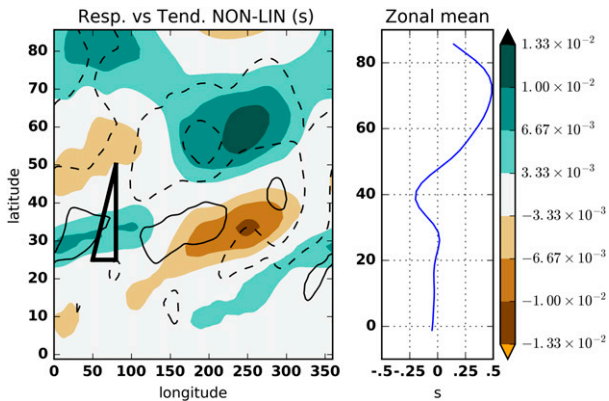
FIG. 10. (left) Linear regression coefficient (colors; s) between the anomalous zonal wind considered pointwise as a function of longitude and latitude and the nonlinear component of the momentum flux convergence computed as in Fig. 9d. Contours indicate the mean response of series N averaged between month 4 and month 12 (drawn at $-1.25, -0.5, 0.5,$ and $1.25 \, \text{m s}^{-1}$). The thick black line indicates the position of the storm-track triangle. (right) Zonal mean of the regression coefficient shown in the left panel.

FIG. 11. Red diamonds indicates the response of the zonal wind at 300 hPa (50°–80°N) in series N plotted vs the climatological jet latitude averaged in the sector where the heating is applied. Black circles show the response of the zonal wind at 300 hPa (50°–80°N) for experiments in series Z (Z0, Za, Zb, Zc) plotted vs the climatological jet latitude averaged zonally. The response is averaged between month 1 and month 12. Bars indicate where the response is not statistically significant at 95% confidence interval according to a t test. Dashed lines are linear fits.

forcing is placed in the Atlantic or in the Pacific. In this view, our results suggest the following interpretation: the stratospheric component (absent in our case) and its impact on the troposphere may change sign according to a different relative position of the heat source, with an intensity modulated by the constructive or destructive interference with climatological stationary waves. The tropospheric component (which dominates in our case) may be systematically a negative NAO/AO whose intensity is modulated, all other things being equal, also by the jet stream latitude in regions of polar heating. This is then to be tested explicitly and put on a stronger basis in targeted experiments with realistic stationary waves and jet latitude.

We have also analyzed radiative effects and cloud feedbacks in our model (not shown), but they do not show an interpretable link with the sensitivity of the response shown in Fig. 7. The area in the proximity of the storm track is particularly sensitive to any rise of temperature in the pole (Fig. 1). Results suggest also that areas where the climatological low-level jet reaches northernmost latitudes are more likely to be sensitive to regional surface forcing. With stationary waves being predicted to change in structure and location in response to climate change (Simpson et al. 2016), it is very likely that the sensitivity of the global circulation to high-latitude forcing will also be changed and potentially magnified (since the stationary waves would extend over areas of higher seasonal temperature variability). The strongest response is found when the heating is near the jet exit, downstream of the storm track. This fact is fairly
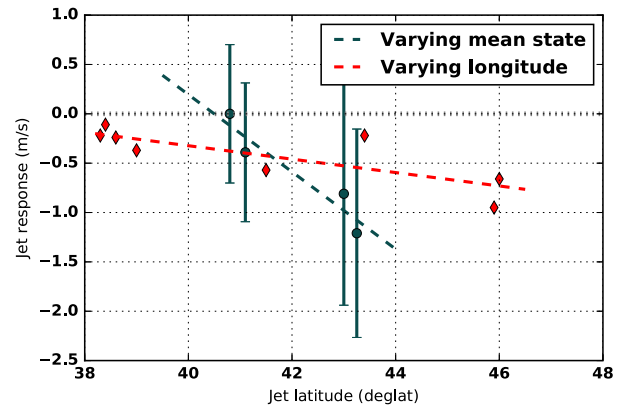
surprising as one could speculate that a modification of the meridional temperature gradient is most effective if in phase with an area of high baroclinicity. The strongest sensitivity to latitudinal shifts is found also in the jet exit region; the sensitivity to longitudinal shifts is remarkably large in the 60°–70°N band, and is absent in lower latitudes. This fact emphasizes the dominant role of linear interference for midlatitude forcing and suggests that nonlinear dynamical feedbacks become crucial for heating in the polar regions. The conjecture of high-snow–low-ice interference that is discussed in Cohen et al. (2014) can be recovered also in our simple model. It is arguable indeed that the hypothesized constructive interference between a high-latitude warming and a midlatitude cooling in the Siberian sector corresponds to the linear combination of the response in Fig. 6f minus the response in Fig. 6a.

Detailed features of the forcing have a strong impact on the outcome of the simulation even in a very simple climate. Our findings, in particular the very high sensitivity of the response to small latitudinal shifts, suggest that studies on the atmospheric response to intensified fluxes in the polar region would increase in robustness if they used a combination of slightly different forcing patterns. Indeed as shown by Fig. 7, a model with a relatively low degree of complexity and a flow that is weakly perturbed from being zonal is able to produce very different responses to very similar forcing patterns. Similarly, it is arguable that the representation of two-way interactions between the atmosphere and the Arctic

surface in coupled models depends strongly and non-uniformly on the biases in the location and intensity of sea ice and sea surface temperature (see, e.g., García-Serrano et al. 2016).

The results also encourage testing of the atmospheric response to polar surface heating combined with other high-latitude forcings that can control the position of the jet on a monthly and subseasonal time scale, such as tropical teleconnections and the stratospheric influence.

The climatological longitude of the collapse of jet latitude over Eurasia may be an important feature to understand multimodel spread that has received little attention so far.

To summarize, the idealized modeling approach used in this study highlights the importance of the geographical location of high-latitude heating for polar–midlatitude teleconnections, and it better defines questions to be addressed in future research. Such questions include the following: Is the atmospheric response more or less sensitive to the vertical structure and nature of the forcing as it is to the location of the forcing? How does this sensitivity manifest itself in more complex models with a seasonal cycle, and more realistic representations of topography, stratosphere, and cloud physics? How exactly does the heating at the downstream part of the storm track induce the strong responses in nonlinear eddy fluxes and the associated shifts in the mean jet? How is this mechanism affected in warmer climates? What is the role of baroclinic and barotropic feedbacks in shaping the response (e.g., Burrows et al. 2017)?

5. Concluding remarks

The response of the atmosphere to extratropical surface forcing has been investigated in a zonally asymmetric aquaplanet climate with a localized storm track. These experiments, despite being unable to capture the full complexity of the observed interaction, are illustrative of the adjustment of the tropospheric jet to surface heating placed in different locations across the mid- and high latitudes. The main findings of this study are enumerated below:

- The mean response to high-latitude heating is a shallow warming in the poleward side of the tropospheric jet, an equatorward displacement of the jet, and a weakening of the westerly flow on the poleward side of the jet. When the heating is placed in the midlatitudes, in correspondence of the core of the jet, the jet response projects onto the opposite pattern.
- The spatial scale of the response ranges from local (synoptic) to hemispheric. The jet response, defined as

the zonal-mean zonal wind response at 300 hPa between 50° and 80°N, has been mapped as a function of the central longitude and latitude of the surface heating. The magnitude of the response ranges from +1 to −1 m s^{-1}, decreasing on average with latitude. The jet response reaches the largest negative value when the heating is placed far downstream with respect to the storm track, at its northernmost extension.

- The sensitivity of the jet response to changes in the central longitude is small when the heating is placed in the midlatitudes or at very high latitudes. It is possible to identify a latitude band (between 60° and 70°N) where a large sensitivity to shifts of the central longitude of the heat source is found.
- A strong response is associated with a reduction of storminess in high latitudes and an equatorward shift of the storm track. Results suggest that the reduced storminess should be explained by changes in their propagation and their strength into the polar environment, and not by changes in their growth rate in the midlatitudes.
- For high-latitude heating, the magnitude of the response is proportional to upper-level momentum convergence by transient eddies. The lack of eddy heat flux response above the tropopause is noticeable. In this case, linear interference between anomalous and climatological waves does not explain the sensitivity to changes in the central longitude of the heating. This is arguably a feature of the simple climate used in this study, with a weak and unrealistic zonally asymmetric mean flow. Nonetheless, it indicates an important role of transient eddies that is not found, for instance, when the heating is placed in the midlatitudes. This finding should be tested in state-of-the-art models. In conjunction with high-end climate models, modeling frameworks at lower complexity can complement the picture, eventually adding statistical robustness and nuances to dynamical mechanisms found in this study.
- The magnitude of the jet response to a zonally symmetric high-latitude forcing is broadly proportional to the climatological latitude of the low-level jet. The magnitude of the jet response to localized heating is proportional to the climatological jet latitude in the heating sector.

The magnitude of the zonal-mean response of the midlatitude jet depends fundamentally on the zonal and meridional coordinates. The area of high baroclinicity of the simple climate is the most responsive, but the strongest zonal-mean response is found when the heating is placed far downstream of this area. The analysis has revealed the high sensitivity of the response to small

changes in the position of the forcing in the jet exit region and this sensitivity is linked to transient eddy feedbacks.

Investigations of high-latitude teleconnections can potentially be more illustrative if slightly different combinations of forcing patterns and atmospheric flows are considered. Exact computations of how atmospheric eddies react to the heating can be crucial to better understand the observed phenomena and to complement the picture offered by linear wave interference. Interestingly, a cautious comparison of this idealized case with Earth's atmosphere indicates a particular efficiency of the Barents–Kara region to warm the polar cap and to produce a stronger than average response in the midlatitudes, also in absence of linear interference between anomalous and climatological waves. This should be assessed in state-of-the-art models. Finally, it can be speculated that the average location of the suppression of the jet latitude over Eurasia and the variability of the jet latitude over the European sector are potential good indicators to investigate the model dependence of the atmospheric response to surface warming in the Nordic seas, the Barents Sea, and the Siberian shelf.

APPENDIX

Linear and Nonlinear Terms

The Eliassen–Palm flux has been defined following Edmon et al. (1980) and

$$F_{(\phi)} = -a\cos\phi\langle u^*v^*\rangle, \quad F_{(p)} = fa\cos\phi\langle \theta^*v^*\rangle/\langle \theta_p\rangle \quad \text{(A1)}$$

are, respectively, the meridional and vertical components, a is the radius of Earth, f is the Coriolis parameter, ϕ is latitude, u and v are, respectively, the zonal and meridional component of the wind, and θ is potential temperature. We denote the zonal mean and deviations from it with angle brackets ($\langle\rangle$) and asterisks (*).

The momentum flux (and similarly the heat flux) for the reference experiment (e.g., CONTROL0 in most cases, labeled with the Ctl subscript) is decomposed into

$$\langle u_{Ctl}^* v_{Ctl}^* \rangle = \langle [U_c^* + u_{Ctl}^{*\prime}(t)][V_c^* + v_{Ctl}^{*\prime}(t)] \rangle$$
$$= \langle U_c^* V_c^* \rangle + \langle u_{Ctl}^{*\prime}(t) V_c^* \rangle + \langle U_c^* v_{Ctl}^{*\prime}(t) \rangle$$
$$+ \langle u_{Ctl}^{*\prime}(t) v_{Ctl}^{*\prime}(t) \rangle \quad \text{(A2)}$$

where $(U_c^*, V_c^*) = (\overline{u_{Ctl}^*}, \overline{v_{Ctl}^*})$ is the climatological flow, the bar indicates temporal and ensemble mean, and the prime indicates deviation from (U_c^*, V_c^*). Similarly for the experiment with additional surface heating (labeled with the "sh" subscript)

$$\langle u_{sh}^* v_{sh}^* \rangle = \langle [U_c^* + u_{sh}^{*\prime}(t)][V_c^* + v_{sh}^{*\prime}(t)] \rangle$$
$$= \langle U_c^* V_c^* \rangle + \langle u_{sh}^{*\prime}(t) V_c^* \rangle + \langle U_c^* v_{sh}^{*\prime}(t) \rangle$$
$$+ \langle u_{sh}^{*\prime}(t) v_{sh}^{*\prime}(t) \rangle. \quad \text{(A3)}$$

Averaging over time, we get

$$\overline{\langle u_{sh}^* v_{sh}^* \rangle} = \langle U_c^* V_c^* \rangle + \langle \Delta U^* V_c^* + U_c^* \Delta V^* \rangle + \overline{\langle u_{sh}^{*\prime}(t) v_{sh}^{*\prime}(t) \rangle}, \quad \text{(A4)}$$

$$\overline{\langle u_{Ctl}^* v_{Ctl}^* \rangle} = \langle U_c^* V_c^* \rangle + \overline{\langle u_{Ctl}^{*\prime}(t) v_{Ctl}^{*\prime}(t) \rangle}, \quad \text{(A5)}$$

where $\overline{u_{sh}^{*\prime}} = \Delta U^*$ and $\overline{v_{sh}^{*\prime}} = \Delta V^*$ are, respectively, the time-mean zonal wind and meridional wind zonally asymmetric response, while $\overline{u_{Ctl}^{*\prime}} = \overline{v_{Ctl}^{*\prime}} = 0$. The anomalous flux can be decomposed into

$$\Delta\overline{\langle u^*v^* \rangle} = \overline{\langle u_{sh}^* v_{sh}^* \rangle} - \overline{\langle u_{Ctl}^* v_{Ctl}^* \rangle}$$
$$= \langle \Delta U^* V_c^* + U_c^* \Delta V^* \rangle + [\overline{\langle u_{sh}^{*\prime}(t) v_{sh}^{*\prime}(t) \rangle}$$
$$- \overline{\langle u_{Ctl}^{*\prime}(t) v_{Ctl}^{*\prime}(t) \rangle}]. \quad \text{(A6)}$$

The first term on the RHS of Eq. (A6) is referred to as the interference term; the second one is the nonlinear term. A 9-day running mean is applied to the time series of u and v to compute the nonlinear term for synoptic frequencies.

The tendency of the zonal wind explained by momentum flux convergence has been computed as

$$(\langle u^*v^* \rangle)_y = -\frac{1}{a\cos^2\phi}\frac{\delta(\langle u^*v^* \rangle \cos^2\phi)}{\delta\phi}. \quad \text{(A7)}$$

The RHS of Eq. (A7) for anomalous momentum flux is used in many figures as an approximation at 300 hPa for the anomalous divergence of the term $[1/(a\cos\phi)]\nabla \cdot F$ in the tendency equation for the zonal-mean zonal wind.

REFERENCES

Barnes, E. A., and J. A. Screen, 2015: The impact of Arctic warming on the midlatitude jet-stream: Can it? Has it? Will it? *Wiley Interdiscip. Rev.: Climate Change*, **6**, 277–286, https://doi.org/10.1002/wcc.337.

Burrows, D. A., G. Chen, and L. Sun, 2017: Barotropic and baroclinic eddy feedbacks in the midlatitude jet variability and responses to climate change–like thermal forcings. *J. Atmos. Sci.*, **74**, 111–132, https://doi.org/10.1175/JAS-D-16-0047.1.

Cohen, J., and Coauthors, 2014: Recent Arctic amplification and extreme mid-latitude weather. *Nat. Geosci.*, **7**, 627–637, https://doi.org/10.1038/ngeo2234.

Deser, C., R. A. Tomas, and S. Peng, 2007: The transient atmospheric circulation response to North Atlantic SST and sea ice anomalies. *J. Climate*, **20**, 4751–4767, https://doi.org/10.1175/JCLI4278.1.

Edmon, H. J., B. J. Hoskins, and M. E. McIntyre, 1980: Eliassen–Palm cross sections for the troposphere. *J. Atmos. Sci.*, **37**, 2600–2616, https://doi.org/10.1175/1520-0469(1980)037<2600:EPCSFT>2.0.CO;2.

García-Serrano, J., and Coauthors, 2016: Multi-model assessment of linkages between eastern Arctic sea-ice variability and the Euro-Atlantic atmospheric circulation in current climate. *Climate Dyn.*, **49**, 2407–2429, https://doi.org/10.1007/s00382-016-3454-3.

Hoskins, B. J., and D. J. Karoly, 1981: The steady linear response of a spherical atmosphere to thermal and orographic forcing. *J. Atmos. Sci.*, **38**, 1179–1196, https://doi.org/10.1175/1520-0469(1981)038<1179:TSLROA>2.0.CO;2.

Kaspi, Y., and T. Schneider, 2013: The role of stationary eddies in shaping midlatitude storm tracks. *J. Atmos. Sci.*, **70**, 2596–2613, https://doi.org/10.1175/JAS-D-12-082.1.

Kucharski, F., F. Molteni, M. P. King, R. Farneti, I.-S. Kang, and L. Feudale, 2013: On the need of intermediate complexity general circulation models: A ''SPEEDY'' example. *Bull. Amer. Meteor. Soc.*, **94**, 25–30, https://doi.org/10.1175/BAMS-D-11-00238.1.

McKenna, C. M., T. J. Bracegirdle, E. F. Shuckburgh, P. H. Haynes, and M. M. Joshi, 2018: Arctic sea ice loss in different regions leads to contrasting Northern Hemisphere impacts. *Geophys. Res. Lett.*, **45**, 945–954, https://doi.org/10.1002/2017GL076433.

Molteni, F., 2003: Atmospheric simulations using a GCM with simplified physical parametrizations. I: Model climatology and variability in multi-decadal experiments. *Climate Dyn.*, **20**, 175–191, https://doi.org/10.1007/s00382-002-0268-2.

Overland, J., and Coauthors, 2016: Nonlinear response of midlatitude weather to the changing Arctic. *Nat. Climate Change*, **6**, 992–999, https://doi.org/10.1038/nclimate3121.

Petoukhov, V. and V. A. Semenov, 2010: A link between reduced Barents-Kara Sea ice and cold winter extremes over northern continents. *J. Geophys. Res.*, **115**, D21111, https://doi.org/10.1029/2009JD013568.

Ruggieri, P., F. Kucharski, R. Buizza, and M. H. P. Ambaum, 2017: The transient atmospheric response to a reduction of sea-ice cover in the Barents and Kara Seas. *Quart. J. Roy. Meteor. Soc.*, **143**, 1632–1640, https://doi.org/10.1002/qj.3034.

Scaife, A. A., and Coauthors, 2014: Skillful long-range prediction of European and North American winters. *Geophys. Res. Lett.*, **41**, 2514–2519, https://doi.org/10.1002/2014GL059637.

Screen, J. A., 2017: Simulated atmospheric response to regional and pan-Arctic sea ice loss. *J. Climate*, **30**, 3945–3962, https://doi.org/10.1175/JCLI-D-16-0197.1.

Sellevold, R., S. Sobolowski, and C. Li, 2016: Investigating possible Arctic–midlatitude teleconnections in a linear framework. *J. Climate*, **29**, 7329–7343, https://doi.org/10.1175/JCLI-D-15-0902.1.

Serreze, M. C., A. P. Barrett, J. C. Stroeve, D. N. Kindig, and M. M. Holland, 2009: The emergence of surface-based Arctic amplification. *Cryosphere*, **3**, 11–19, https://doi.org/10.5194/tc-3-11-2009.

Simmons, A. J., J. M. Wallace, and G. W. Branstator, 1983: Barotropic wave propagation and instability, and atmospheric teleconnection patterns. *J. Atmos. Sci.*, **40**, 1363–1392, https://doi.org/10.1175/1520-0469(1983)040<1363:BWPAIA>2.0.CO;2.

Simpson, I. R., R. Seager, M. Ting, and T. Shaw, 2016: Causes of change in Northern Hemisphere winter meridional winds and regional hydroclimate. *Nat. Climate Change*, **6**, 65–70, https://doi.org/10.1038/nclimate2783.

Smith, D. M., N. J. Dunstone, A. A. Scaife, E. K. Fiedler, D. Copsey, and S. C. Hardiman, 2017: Atmospheric response to Arctic and Antarctic sea ice: The importance of ocean–atmosphere coupling and the background state. *J. Climate*, **30**, 4547–4565, https://doi.org/10.1175/JCLI-D-16-0564.1.

Smith, K. L., C. G. Fletcher, and P. J. Kushner, 2010: The role of linear interference in the annular mode response to extratropical surface forcing. *J. Climate*, **23**, 6036–6050, https://doi.org/10.1175/2010JCLI3606.1.

Sun, C., F. Kucharski, J. Li, F.-F. Jin, I.-S. Kang, and R. Ding, 2017: Western tropical Pacific multidecadal variability forced by the Atlantic multidecadal oscillation. *Nat. Commun.*, **8**, 15998, https://doi.org/10.1038/ncomms15998.

Sun, L., C. Deser, and R. A. Tomas, 2015: Mechanisms of stratospheric and tropospheric circulation response to projected Arctic sea ice loss. *J. Climate*, **28**, 7824–7845, https://doi.org/10.1175/JCLI-D-15-0169.1.

Voigt, A., and Coauthors, 2016: The Tropical Rain Belts with an Annual Cycle and a Continent Model Intercomparison Project: TRACMIP. *J. Adv. Model. Earth Syst.*, **8**, 1868–1891, https://doi.org/10.1002/2016MS000748.

Walker, G. T., 1925: Correlation in seasonal variations of weather—A further study of world weather. *Mon. Wea. Rev.*, **53**, 252–254, https://doi.org/10.1175/1520-0493(1925)53<252:CISVOW>2.0.CO;2.

Wallace, J. M., and D. S. Gutzler, 1981: Teleconnections in the geopotential height field during the Northern Hemisphere winter. *Mon. Wea. Rev.*, **109**, 784–812, https://doi.org/10.1175/1520-0493(1981)109<0784:TITGHF>2.0.CO;2.

Woollings, T., A. Hannachi, and B. Hoskins, 2010: Variability of the North Atlantic eddy-driven jet stream. *Quart. J. Roy. Meteor. Soc.*, **136**, 856–868, https://doi.org/10.1002/qj.625.

Zappa, G., and T. G. Shepherd, 2017: Storylines of atmospheric circulation change for European regional climate impact assessment. *J. Climate*, **30**, 6561–6577, https://doi.org/10.1175/JCLI-D-16-0807.1.

Zhang, P., Y. Wu, and K. L. Smith, 2018: Prolonged effect of the stratospheric pathway in linking Barents–Kara Sea sea ice variability to the midlatitude circulation in a simplified model. *Climate Dyn.*, **50**, 527–539, https://doi.org/10.1007/s00382-017-3624-y.